

Geometry and charge carrier induced stability in Casimir actuated nanodevices

R. Esquivel-Sirvent^a and R. Pérez-Pascual

Instituto de Física, Universidad Nacional Autónoma de México, Apartado Postal 20-364, México D.F. 01000, Mexico

Received 22 August 2013 / Received in final form 27 September 2013

Published online (Inserted Later) – © EDP Sciences, Società Italiana di Fisica, Springer-Verlag 2013

Abstract. In this work we demonstrate, that in Casimir actuated nanodevices, geometry and charge carriers concentration change the stability and the pull-in conditions that cause stiction. The stability is analyzed by calculating the bifurcation diagram of the capacitive switch as a function of plate thickness for Au and Si showing that previous calculations based on Lifshitz formula for half-spaces underestimated the stability conditions. Taking into account the size effect, we recalculate the bifurcation diagram for different metals and for Si with different carrier concentrations showing the change in the stability conditions.

1 Introduction

Casimir [1] predicted that two neutral parallel plates made of perfect conductors will attract each other with a force that depends only on fundamental constants and varies as the inverse fourth power of their separation. Lifshitz and collaborators [2,3], showed that for real materials the force will depend on the dielectric properties of the plates. The Casimir force has been measured with high precision using a variety of techniques such as atomic force microscopy, torsional balances and microelectromechanical systems [4–13].

The stability of micro and nano electromechanical devices (MEMS and NEMS) is influenced by the Casimir force as shown by Serry et al. [14] and Buks and Roukes [15], causing stiction, that renders these devices useless [16]. The role of Casimir and van der Waals forces in the stiction and actuation of MEMS and NEMS has been studied by several authors [17–25]. The Casimir interaction and stability in MEMS and NEMS can be further complicated by the presence of surface roughness [24,26–28]. Additionally, even with well grounded devices, residual potentials or patch potentials can add additional parasitic forces. This has been an important issue in the interpretation of Casimir force experiments [29,30].

To avoid the unwanted stiction effect due to the Casimir force, several schemes have been proposed such as the use of curved surfaces, materials with very low dielectric functions (aerogels) [31], application of external magnetic fields in semiconductors that can support magneto plasmons [32] and the use of topological insulators [33]. The possibility of using a non-monotonic change in the force, from attractive to repulsive, to inhibit stiction was proposed by Bostrom et al. [34].

The studies on the influence of the Casimir force in MEMS and NEMS usually assumes semi-infinite plates

rather than more realistic finite thickness ones. This is accurate for metallic plates with a thickness larger than their plasma wavelength. However, for smaller plates, the thickness plays an important role in the calculation of the van der Waals and Casimir forces. Pirozhenko and Lambrecht [35] calculated the influence of slab thickness in the Casimir force between thin silicon plates with different concentration of carriers. A similar study was done for thin films grown by sputtering that exhibit an insulator-metallic transition as the thickness increases [36]. The correction to the Casimir force between films of a few atomic layers was recently calculated by Bostrom et al. [37], even down to one atomic layer deposits. Another effect relevant for thin layers is the nonlocal behavior (spatial dispersion) of the dielectric function. However, as shown in reference [38] the difference in the Casimir force between the local and nonlocal calculation is of a few tenths of a percent.

In this paper we present a theoretical calculation of the influence of plate thickness in micro and nano mechanical systems actuated by dispersive forces. In particular we show that the stability conditions have been overestimated and that the plate thickness can be used as an additional design parameter. Also we consider the role of the plasma frequency in the stability conditions using different metals and doped Si with varying charge carrier concentrations. Without loss of generality, in this work we focus only on the Casimir force and do not consider other forces of electrostatic origin.

2 Casimir force between finite thickness plates

The Casimir force between two parallel plates of thickness D , local dielectric function ϵ , surface area S and

^a e-mail: raul@fisica.unam.mx

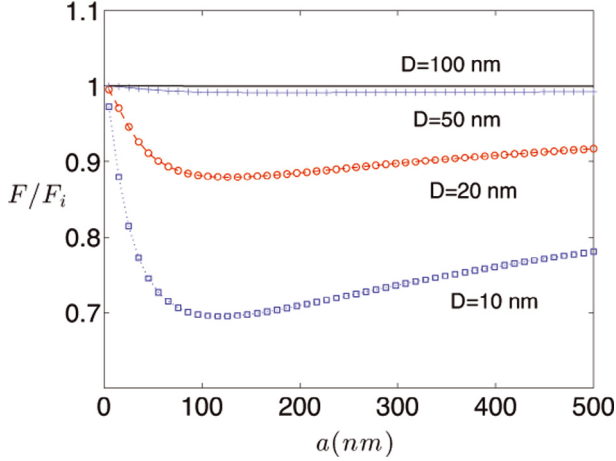


Fig. 1. Force between two Au plates normalized to the force between semi-infinite plates F/F_i as a function of the separation a of the plates and their thickness D . As expected, when the plate thickness approaches the plasma wavelength of Au, $F/F_i \rightarrow 1$.

separation a is given by [2,3]:

$$F(a) = \sum_{p=\perp,||} \frac{\hbar S}{2\pi^2} \int_0^\infty \int_0^\infty k f(\omega, k) Q dQ d\omega, \quad (1)$$

where the sum is over the two light polarizations (parallel and perpendicular) and

$$f(\omega, k) = \frac{r_p^2}{e^{2ka} - r_p^2}. \quad (2)$$

The wave vector component perpendicular to the plates is $k = \sqrt{(\omega/c)^2 + Q^2}$, and Q is the wave vector along the plates. The reflectivities r_p are those of the finite width plates, and are given by [35]:

$$r_p = r_{pF} \frac{1 - e^{-2\delta}}{1 - r_{pF} e^{-2\delta}}, \quad (3)$$

where $\delta = D\sqrt{\frac{\omega^2}{c^2}(\epsilon(i\omega) - 1) + k^2}$ and r_{pF} are the Fresnel coefficients.

The frequency integral in equation (1) is done along the imaginary axis $i\omega$, thus the dielectric functions become $\epsilon(\omega) \rightarrow \epsilon(i\omega)$. The Casimir force given by equation (1) does not include temperature effects that only become relevant at large separations. With the separation range considered in this paper, the difference in the force is of a few percent.

The effect of the plate thickness on the force is shown in Figure 1 for two plates of Au and in Figure 2 for plates made of intrinsic Si. In both figures we plot the force calculated for plates of thickness D divided by the force for half-spaces ($D \rightarrow \infty$) as a function of plate separation. For a thickness of $D = 100$ nm we observe that the Au plate can be regarded as a half-space and in the case of Si the force is much smaller than for the half-space.

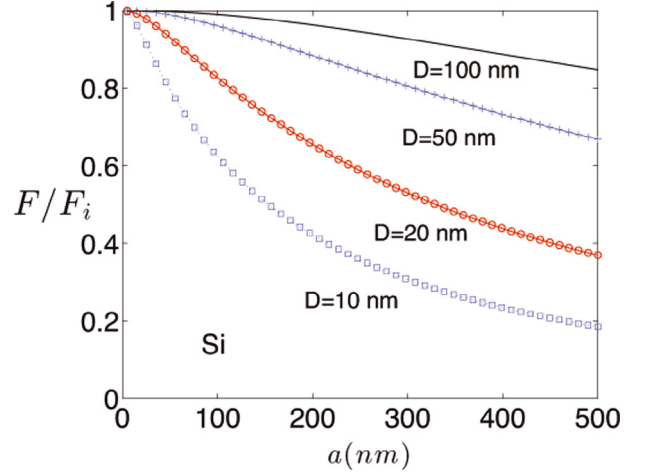


Fig. 2. Force between two Si plates normalized to the force between semi-infinite plates F/F_i as a function of the separation a of the plates and their thickness D .

For ease of calculation we use an analytic expression for the dielectric function of Au that fits the experimental data well into the frequency range of the inter-band transitions [39,40]. Alternatively one can use directly the experimental dielectric function of Au as reported by Palik [41]. In both cases, the dielectric function is given for bulk materials and the finite size effect of the system has to be quantified. For a plate of thickness D , the measured dielectric functions ϵ_{bulk} have to be modified as [42]:

$$\epsilon(\omega) = \epsilon_{bulk} + \frac{\omega_p^2}{\omega^2 + i\omega\gamma_0} - \frac{\omega_p^2}{\omega^2 + i\omega(\gamma_0 + v_f/D)}, \quad (4)$$

where ω_p is the plasma frequency, γ_0 is the damping factor and v_f is the Fermi velocity of Au. In the damping the finite size effects come into play. For this reason, we use the Drude model to extrapolate the dielectric function to low frequencies (for a discussion on the issues of using the Drude or the Plasma model at low frequencies when calculating the Casimir force, see Refs. [29,43,44]). The finite size correction is relevant at small frequencies as shown in Figure 3, where we plot the real and imaginary part of the dielectric function of Au for different plate thickness. The experimental data from Palik [41] is plotted with the finite size correction included.

For intrinsic Si the Lorentz model is used [35,45–48], which is approximated by

$$\epsilon(\omega) = \epsilon_\infty + \frac{\omega_0(\epsilon_{st} - \epsilon_\infty)}{\omega_0^2 - \omega^2 - i\gamma\omega}, \quad (5)$$

where ω_0 is a resonant frequency associated to atomic transitions, ϵ_∞ is the high frequency limit of the dielectric constant, and $\epsilon_{st} = \epsilon(\omega = 0)$ is the static dielectric constant. The parameters for Si, as determined from known data are $\epsilon_{st} = 11.68$, $\epsilon_\infty = 1$, $\gamma = 9.859 \times 10^{12} \text{ s}^{-1}$ and $\omega_0 = 5.02 \times 10^{15} \text{ s}^{-1}$ [45].

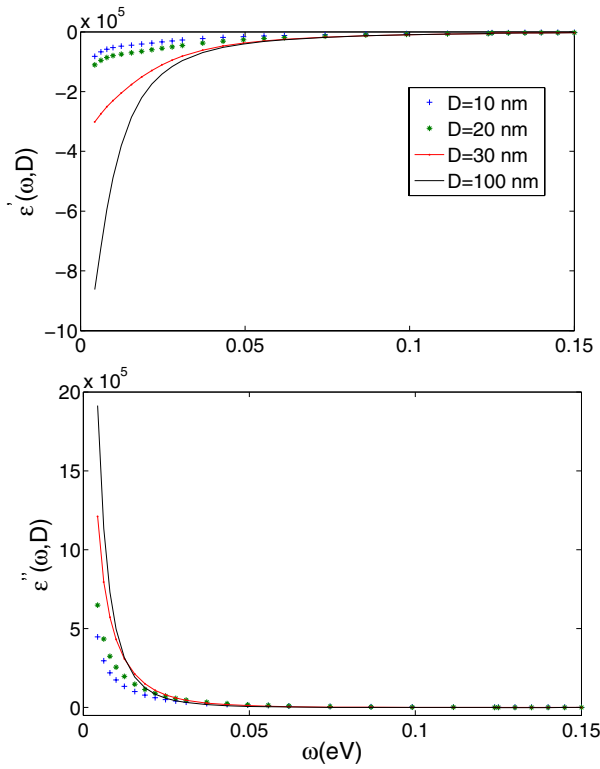


Fig. 3. Real and imaginary part of the dielectric function of Au including finite size corrections for different values of the plate thickness D . For small frequencies the effect becomes more relevant. Again, for values of D close to the plasma wavelength the dielectric function of the plates is that of the bulk values.

3 The model system

We consider a simple lumped system modeled by a capacitive switch. The switch consists of two parallel plates, one fixed and one attached to a linear spring of constant κ and rest position L . The equation of motion for the moving plate is:

$$m \frac{d^2 z}{dt^2} = \kappa(L - z) - F_C(z), \quad (6)$$

where m is the mass of the plate and $z(t)$ is the separation between the plates.

Making the change of variables $y = 2kz$, $\bar{Q} = 2zQ$, $\bar{D} = D/z$ and introducing the characteristic frequency $\bar{\omega} = 2z\omega/c$, the Casimir force (Eq. (1)) can be conveniently written as:

$$\begin{aligned} F_C(z) &= \frac{\hbar c \pi^2 S}{240 z^4} \left(\frac{240}{32 \pi^2} \right) \int_0^\infty \bar{Q} d\bar{Q} \int_0^\infty d\bar{\omega} y f(\bar{\omega}, y), \\ &= \frac{\hbar c \pi^2 S}{240 z^4} \eta(\epsilon(\bar{\omega}), \bar{D}) = F_0 \eta(\epsilon(\bar{\omega}), \bar{D}), \end{aligned} \quad (7)$$

where $F_0 = \hbar c \pi^2 S / 240 z^4$ is the Casimir force for perfect conductors and the function $\eta(\epsilon(\bar{\omega}), \bar{D})$ has the information on the dielectric properties of the plate and their thickness. Clearly if $\eta(\epsilon(\bar{\omega})) \rightarrow 1$ the force between two perfect conductors is recovered in equation (5).

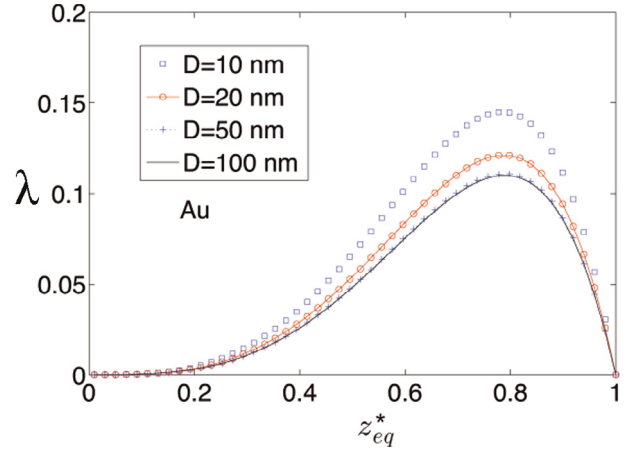


Fig. 4. Relation between the parameter λ and the equilibrium points z_{eq}^* for Au plates of different thicknesses. The points $z_{eq}^* > z_{in}^*$ are stable, where z_{in}^* is the separation corresponding to the maximum of the curves.

Following the standard procedure [28,49] we introduce the dimensionless variables $t^* = t\sqrt{\kappa/m}$ and $z^* = z/L$. The equation of motion, equation (4), can be written as

$$\frac{d^2 z^*}{dt^{*2}} = (1 - z^*) - \frac{\lambda \eta(\epsilon(\bar{\omega}), \bar{D})}{z^{*4}}, \quad (8)$$

where

$$\lambda = \frac{1}{\kappa L} \frac{\hbar c \pi^2 S}{240 L^4}, \quad (9)$$

is the bifurcation parameter that relates the Casimir force (for ideal conductors) at maximum separation with the maximum elastic force (when the plates are in contact). This particular choice of the bifurcation parameter allows us to compare with the ideal conductor case. For large values of the spring constant, the elastic force dominates and periodic solutions of equation (6) are expected. Otherwise, the Casimir force will dominate and the plates will jump to contact. The sets of values for which equilibrium points exist are obtained by setting equation (6) equal to zero to obtain:

$$\lambda = \frac{(1 - z^*) z^{*4}}{\eta(\epsilon(\bar{\omega}), \bar{D})}. \quad (10)$$

3.1 Effect of thickness on the stability

To study the stability of the Casimir actuated MEMS and NEMS, we plot in Figure 4 the parameter λ as a function of separation z^* for Au and Si (Fig. 5) for different values of the plate thickness D . The maximum values of the curves occur at a separation z_{in}^* , that is the pull-in separation. When the separation of the plates is $z^* > z_{in}^*$ the solutions are stable, otherwise we have unstable equilibrium points and the system jumps to contact. In both figures we see that for smaller values of D , the maximum value of λ is larger, and for all cases the maximum value for Au are always smaller than for Si. This is shown in Figure 6 for the Au and Si plates.

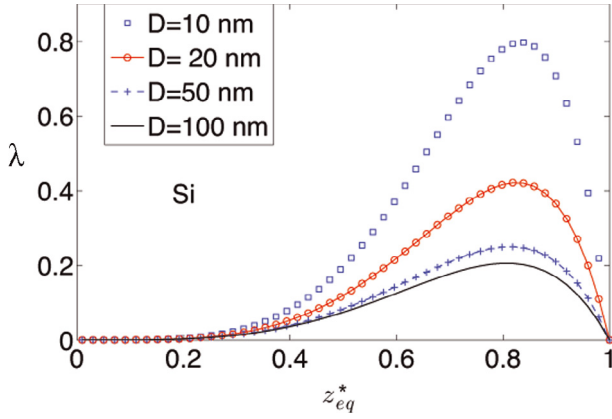


Fig. 5. Same as Figure 4 but for Si plates. Given that the Casimir force between the Si plates is smaller, bigger values of λ_{\max} can be obtained.

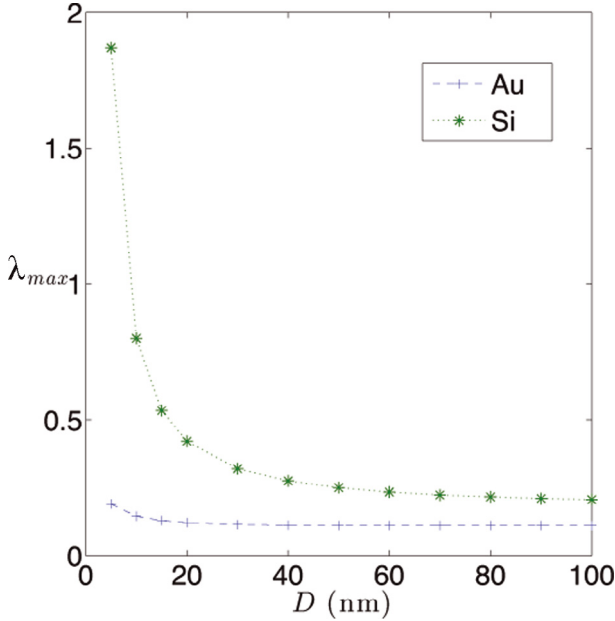


Fig. 6. The maximum values of λ for Au and Si are plotted as a function of plate thickness. The smaller the force, the larger value of λ_{\max} that can be achieved, allowing for the use of softer springs.

The values of λ are related to the spring constant κ as shown in equation (7). The fact that the maximum values of λ for Si are larger at a fixed plate thickness than those of Au, means that given an equilibrium point z^* , $\lambda_{\text{Si}} > \lambda_{\text{Au}}$, thus $\kappa_{\text{Si}} < \kappa_{\text{Au}}$. The same is true if we analyze the Au curves. The thinner the plate the larger the parameter λ at a given separation, meaning that softer spring constants can be used in the design of the devices. For comparison, in Figure 7, we plot the effective stiffness of the spring at the pull-in position z_{in}^* . As the thickness of the plates decreases, the system becomes less stiff. The same behavior is observed for both Au and Si. The stability of the capacitive switch can also be understood considering that the attractive force between the plates changes the resonant frequency of the spring. Introducing

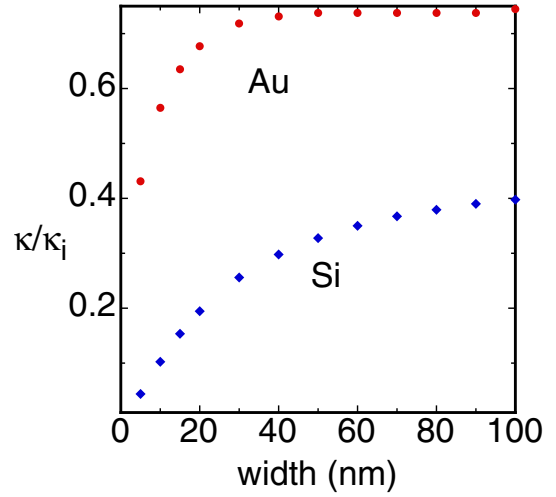


Fig. 7. Changes in the effective stiffness of the system at the pull-in position z_{in}^* . As the thickness of the plates decreases the stiffness of the system decreases as well. The same is observed for both Au and Si. In this figure κ_i is the stiffness if the plates were made of a perfect conductors.

a small displacement z' around an equilibrium point we have displacement $z = z_{eq} + z'$. Replacing in the equation of motion equation (4) and expanding the equation around $z'/z_{eq} \ll 1$ we obtain [50],

$$\begin{aligned} m \frac{d^2 z'}{dt^2} &= -\kappa \left(1 - \frac{4\lambda\eta(\epsilon(\bar{\omega}), \bar{D})}{z_{eq}^5} \right) z' \\ &= -\kappa_{eff} z', \end{aligned} \quad (11)$$

where κ_{eff} is the effective stiffness. Thus, the resonant frequency is now $\omega_{eff} = \sqrt{\kappa_{eff}/m}$. For the stable equilibrium points $z_{eq} > z_{in}$ the frequency is real and in the region of unstable equilibrium it becomes purely imaginary.

3.2 Carrier concentration

For different metals we can calculate the stability points and find the curve of λ vs. z^* . We use a Drude model characterized by the plasma frequency and the damping for the dielectric function of metals (Fig. 8). The inset shows λ_{\max} for the different values of the plasma frequency. In this figure the equilibrium position is $L = 500$ nm.

The dielectric behavior of doped Si plates can be changed. Ginn et al. [51] recently examined the optical properties of heavily-doped Si in particular in the long infrared wavelength to explore its use as a plasmonic materials. The properties were measured using ellipsometry and fitted to a Drude like model. In this case, adding charge carriers by doping Si will change the dielectric function $\epsilon(i\omega)_{Si}$ by having an additional Drude-like term due to the extra carriers [35]. That is:

$$\epsilon(i\omega)_D = \epsilon(i\omega)_{Si} + \frac{\omega_p^2}{\omega(\omega + \gamma)}, \quad (12)$$

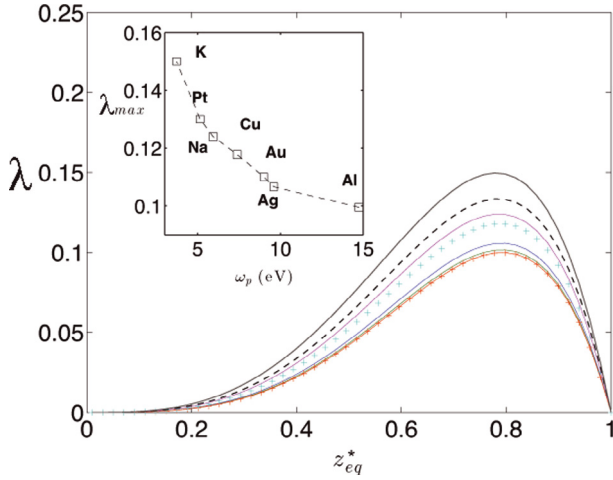


Fig. 8. Bifurcation diagram for plates made of different materials. From top to bottom each curve corresponds to: K, Pt, Na, Cu, Au, Ag, Al. The inset shows the λ_{max} as a function of plasma frequency. In the figure and the inset we assume that the plates have a thickness of $d = 60$ nm and that $L = 500$ nm.

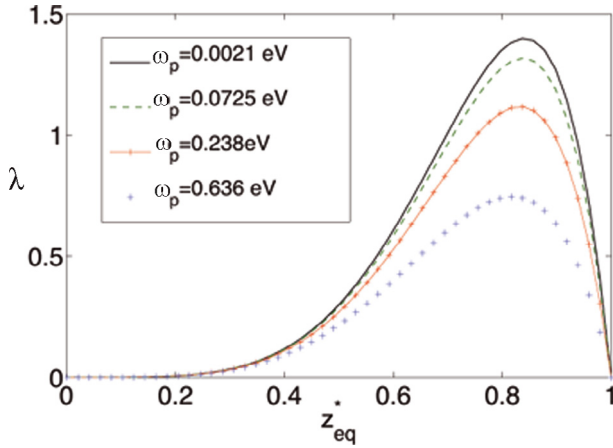


Fig. 9. Equilibrium points for plates made of doped Si, for different dopant concentrations that changes the plasma frequency. As in Figure 8 we assume that the plates have a thickness of $d = 60$ nm and that $L = 5 \mu\text{m}$. The carrier concentration (in units of cm^{-3}) for the different plasma frequencies are [35]: $N = 1.1 \times 10^{15}$ ($\omega_p = 0.0021$ eV), $N = 1.3 \times 10^{18}$ ($\omega_p = 0.0725$ eV), $N = 1.4 \times 10^{19}$ ($\omega_p = 0.238$ eV), $N = 1 \times 10^{20}$ ($\omega_p = 0.636$ eV).

where the carrier concentration N enters in the plasma frequency $\omega_p^2 = 4\pi N e^2 / m^*$, where m^* is the effective mass. In Figure 9, we plot λ as a function of z^* for different doped Si plates. The case of intrinsic Si coincides with the curve for $\omega_p = 0.0021$ eV ($N = 1.1 \times 10^{15} \text{ cm}^{-3}$). As the carrier concentration increases the sample becomes “more metallic”, increasing the value of the dielectric function and thus increasing the Casimir force. In this figure initial separation of the plates is $L = 5 \mu\text{m}$. As shown in reference [35] at large separations between the plates the difference in the Casimir force for the different carrier concentrations becomes more relevant.

4 Conclusions

Unlike electrostatic forces, dispersive forces depend on the thickness of the plates. The usual treatment of the van der Waals interaction in MEMS and NEMS assumes as valid the Casimir force for half-spaces. The finite width of the plates decreases the Casimir interaction, making the system more stable. Thus, the plate thickness can be used as a control parameter in the design of devices where dispersive interactions are important. Furthermore, by properly choosing the plate width, the spring constant can be reduced without having a jump-to-contact or pull-in. Another stability control is the plasma frequency of the plates. This is more clearly seen for the Si plates where the dielectric function is changed by doping and changing the charge carrier density. As the density of carriers increases a more metallic behavior occurs increasing the magnitude of the Casimir force, changing the stability conditions. As shown by Broer et al. [28] the roughness of the plates also plays an important role in the stability. Thus, roughness, dielectric properties and plate thickness expand the space of design parameters to control the stability of MEMS and particularly NEMS for which dispersive forces become more relevant.

R.E-S. acknowledges the partial support of DGAPA-UNAM Project No. IN105612.

References

1. H.B.G. Casimir, Proc. Kon. Ned. Akad. Wet. **51**, 793 (1948)
2. E.M. Lifshitz, Sov. Phys. J. Exp. Theor. Phys. **2**, 73 (1956)
3. I.D. Dzyaloshinskii, E.M. Lifshitz, L.P. Pitaevskii, Usp. Fiz. Nauk **73**, 381 (1961) [Soviet Phys. Usp. **4**, 153]
4. S.K. Lamoreaux, Phys. Rev. Lett. **78**, 5 (1997)
5. S.K. Lamoreaux, Phys. Rev. Lett. **81**, 5475 (1998)
6. U. Mohideen, A. Roy, Phys. Rev. Lett. **81**, 4549 (1998)
7. R.S. Decca, D. López, E. Fischbach, D.E. Krause, Phys. Rev. Lett. **91**, 050402 (2003)
8. G. Bressi, G. Carugno, R. Onofrio, G. Ruoso, Phys. Rev. Lett. **88**, 041804 (2002)
9. D. Iannuzzi, M. Lisanti, F. Capasso, Proc. Natl. Acad. Sci. USA **101**, 4019 (2004)
10. S.K. Lamoreaux, Phys. Rev. A **59**, R3149 (1999)
11. F. Chen, U. Mohideen, G.L. Klimchitskaya, V.M. Mostepanenko, Phys. Rev. A **74**, 022103 (2006)
12. F. Chen, G.L. Klimchitskaya, V.M. Mostepanenko, U. Mohideen, Phys. Rev. Lett. **97**, 170402 (2006)
13. H.B. Chan, Y. Bao, J. Zou, R.A. Cirelli, F. Klemens, W.M. Mansfield, C.S. Pai, Phys. Rev. Lett. **101**, 030401 (2008)
14. F.M. Serry, D. Walliser, J.G. Maclay, J. Microelectromech. Syst. **4**, 193 (1995)
15. E. Buks, M.L. Roukes, Europhys. Lett. **54**, 220 (2001)
16. W.H. Lin, Y.P. Zhao, Microsys. Technol. **11**, 80 (2005)
17. W.H. Lin, Y.P. Zhao, Sensors **7**, 3012 (2007)
18. W.H. Lui, Y.P. Zhao, J. Phys. D **40**, 1649 (2007)
19. R.C. Batra, M. Porfiri, D. Spinello, Eur. Phys. Lett. **77**, 20010 (2007)
20. R.C. Batra, M. Porfiri, D. Spinello, Sensors **8**, 1048 (2008)

21. R.C. Batra, M. Porfiri, D. Spinello, *Int. J. Solids Struct.* **45**, 3558 (2008)
22. R.C. Batra, M. Porfiri, D. Spinello, *J. Sound Vib.* **315**, 939 (2008)
23. F. Pinto, *J. Phys. A* **41**, 164033 (2008)
24. F.W. del Rio, M.P. de Boer, J.A. Knapp, E.D. Reedy Jr., P.J. Clews, M.L. Dunn, *Nat. Mater.* **4**, 629 (2005)
25. J. Zou, Z. Marcet, A.W. Rodriguez, M.T.H. Reid, A.P. McCauley, I.I. Kravchenko, T. Lu, Y. Bao, S.G. Johnson, H.B. Chan, *Nat. Commun.* **4**, 1845 (2013)
26. G. Palasantzas, V.B. Svetovoy, P.J. van Zwol, *Int. J. Mod. Phys. B* **24**, 6013 (2010)
27. W. Broer, G. Palasantzas, J. Knoester, V.B. Svetovoy, *Phys. Rev. B* **85**, 155410 (2012)
28. W. Broer, G. Palasantzas, J. Knoester, V.B. Svetovoy, *Phys. Rev. B* **87**, 125413 (2013)
29. A.O. Sushkov, W.J. Kim, D.A.R. Dalvit, S.K. Lamoreaux, *Nat. Phys.* **7**, 230 (2011)
30. R.O. Behunin, Y. Zeng, D.A.R. Dalvit, S. Reynaud, *Phys. Rev. A* **86**, 052509 (2012)
31. R. Esquivel-Sirvent, *J. Appl. Phys.* **102**, 034307 (2007)
32. R. Esquivel-Sirvent, G.H. Cocoletzi, M. Palomino-Ovando, *J. Appl. Phys.* **108**, 114101 (2010)
33. J.C. Martinez, M.B.A. Jalil, *J. Appl. Phys.* **113**, 204302 (2013)
34. M. Bostrom, S.A. Ellingsen, I. Brevik, M.F. Dou, C. Persson, Bo.E. Sernelius, *Eur. Phys. J. B* **85**, 377 (2012)
35. I. Pirozhenko, A. Lambrecht, *Phys. Rev. A* **77**, 013811 (2008)
36. R. Esquivel-Sirvent, *Phys. Rev. A* **77**, 042107 (2008)
37. M. Bostrom, C. Person, Bo.E. Sernelius, *Eur. Phys. J. B* **86**, 43 (2013)
38. R. Esquivel-Sirvent, V.B. Svetovoy, *Phys. Rev. B* **72**, 045443 (2005)
39. P.G. Etchegoin, E.C. Le Rue, M. Meyer, *J. Chem. Phys.* **125**, 164705 (2006)
40. P.G. Etchegoin, E.C. Le Rue, M. Meyer, *J. Chem. Phys.* **127**, 189901 (2007)
41. E.D. Palik, *Handbook of Optical Constants of Solids* (Academic Press, California, 1998)
42. E.A. Coronado, G.C. Schatz, *J. Chem. Phys.* **119**, 3926 (2003)
43. M. Bostrom, B. Sernelius, *Phys. Rev. Lett.* **84**, 4757 (2000)
44. M. Bordag, G.L. Klimchitskaya, U. Mohideen, V.M. Mostepanenko, *Advances in the Casimir Effect* (Oxford University Press, London, 2009)
45. S. Adachi, *Optical Constants of Crystalline and Amorphous Semiconductors* (Kluwer Academic Publishers, Massachusetts, 1999)
46. R. Esquivel-Sirvent, C. Villarreal, W.L. Mochán, G.H. Cocoletzi, *Phys. Stat. Sol. B* **230**, 409 (2002)
47. H.R. Philipp, E.A. Taft, *Phys. Rev.* **120**, 37 (1960)
48. L. Duraffourg, P. Andreucci, *Phys. Lett. A* **359**, 406 (2006)
49. J.A. Pelesko, D.H. Bernstein, *Modeling MEMS and NEMS* (Chapman & Hall/CRC, Boca Raton, 2003)
50. V. Rochus, D.J. Rixen, J.C. Golinval, *Nonlinear Analysis* **63**, e1619 (2005)
51. J.C. Ginn, R.L. Jarecki, E.A. Shaner, P.S. Davids, *J. Appl. Phys.* **110**, 043110 (2011)